December 1999

Minijets and Transverse Energy Flow in High Energy Collisions

Gösta Gustafson[1] and Gabriela Miu[2]

Department of Theoretical Physics,
Lund University, Lund, Sweden

Abstract

We study the distribution of jets and transverse energy flow in high energy hadron-hadron or nucleus-nucleus collisions. In the minijet region correlations and coherence effects can be taken into account in a description, where the parton flux is described by non-integrated structure functions. In a "naive" calculation based on integrated structure functions, the cross section blows up for small $p_\perp$, which makes it necessary to introduce a soft cutoff. In our approach we find a dynamical suppression at low $p_\perp$, which makes it possible to extrapolate to higher energies and make more reliable predictions for RHIC and LHC.

[1]gosta@thep.lu.se
[2]gabriela@thep.lu.se

1 Introduction

With increasing energies in hadron-hadron or nucleus-nucleus collisions, the cross section for hard subcollisions increases and becomes more and more important. The amount of minijets and transverse energy becomes essential for understanding the background in searches for new particles or new phenomena at the LHC as well as for the "initial conditions" in nucleus-nucleus collisions. In calculations of the flow in either a quark-gluon plasma or a hadronic phase, the results are very sensitive to the properties of the initial parton state which resulted from a large number of hard subcollisions. Thus a reliable estimate of these initial conditions is essential for the interpretation of signals from a possible plasma formation in experiments at RHIC or LHC.

At high $q_\perp$ the jet cross section can be described by a product of structure functions describing the flux of partons and the cross section for a hard partonic subcollision. Symbolically we write (cf. Fig. 1)

$$\frac{d\sigma}{dq_\perp^2} \sim F(x_1, q_\perp^2)\, F(x_2, q_\perp^2)\, \frac{d\hat{\sigma}}{dq_\perp^2}. \tag{1}$$

This is a relevant description when $q_\perp$ is so large that the structure functions can be described by DGLAP evolution, i. e. by $k_\perp$-ordered chains from the incoming hadrons towards the hard collision. For smaller $q_\perp^2$ and/or larger energies (which implies smaller x-values) we enter the BFKL region, in which non-ordered chains are important. As we will discuss in detail below, the expression in eq. (1) will then significantly overestimate the cross section. In order to agree with experimental data for $E_\perp$-flow, many calculations based on eq. (1) introduce a cutoff for small $q_\perp$. This implies, however, that it is difficult to make predictions for higher energies. Without a dynamical understanding of the origin of the overestimate, it is not possible to judge how an effective cutoff should vary with energy.

When $q_\perp$ becomes smaller, it is not enough to understand the properties of the structure function F in the BFKL region. When non-ordered chains become important there is not a unique link which has a dominating $k_\perp$. There may be several links in a single chain, which can be regarded as a hard collision, and we must understand the correlations between such subcollisions. Actually, in eq. (1) every link in Fig. 1 gives a contribution which corresponds to one subcollision between two partons. Thus the number of emitted partons described by eq. (1) is twice the number of links, while in reality the number of produced partons in Fig. 1 equals the number of links in the chain. Consequently we must find a way to avoid double counting, and we must also take into account the modifications to the cross section, when the virtuality of the colliding partons may be larger than the momentum transfer between them.

A formalism for DIS which interpolates between the DGLAP and BFKL regions, and which describes both the cross section and the final state properties, was developed by Ciafaloni, Catani, Fiorani, and Marchesini [1]. The Linked Dipole Chain (LDC) model [2, 3] is a reformulation and generalization of the CCFM formalism. It can within a single formalism describe different types of events, "normal DIS", boson-gluon fusion events, and events with hard subcollisions in resolved photon events. For such a resolved photon event the result can be interpreted as evolutions from both the proton and the photon ends towards a hard parton-parton collision. This feature implies that the LDC model is also suitable for a description of hard collisions in hadronic interactions.

The fact that the LDC formalism is symmetric with respect to evolution from the

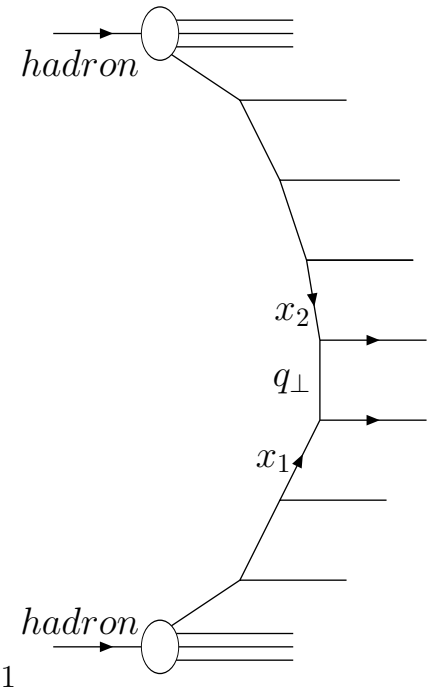

Figure 1: *A fan diagram for a hadron-hadron collision.*

target or the projectile end, makes it suitable to describe the correlated subcollisions corresponding to a long chain, with possibly more than one maximum. The result is that the minijet cross section can be simply expressed in terms of the *non-integrated* structure functions, as is consistent with $k_\perp$-factorization. For large $q_\perp$ the result agrees with the result obtained from eq. (1), but for smaller $q_\perp$ we find a dynamical suppression, which implies that the $E_\perp$-flow in the minijet region is reduced by roughly a factor of 2. This implies that the strong sensitivity upon the soft cutoff in a "naive" approach is essentially reduced.

It is well known that the BFKL formalism with a constant coupling, α_s, implies that the transverse momenta grow like a random walk in y or in $\ln 1/x$ (what is called Bartels' cigar). For a running α_s we obtain instead a saturation of the $k_\perp$-distribution [3]. Therefore very large chains develop a central plateau in rapidity. This means that with increasing beam energy the transverse energy density in each chain will stay limited, although the total $dE_\perp/dy$ will increase as the number of possible chains grows with energy.

2 DIS

A deep inelastic scattering event is generally described in terms of a fan diagram as shown in Fig 2. Here q_i denote quasireal partons emitted as initial state radiation, while the links k_i are virtual. The dashed lines denote final state emission, which is assumed to be emitted without changing the cross section and with negligible recoils for the emitting partons q_i.

In the large Q^2 region, the DGLAP region, the dominant contributions come from ordered chains which satisfy $Q^2 > k^2_{\perp,n} > ... > k^2_{\perp,i} > k^2_{\perp,i-1}$ and $k_{+,i} > k_{+,i+1}$. Each such

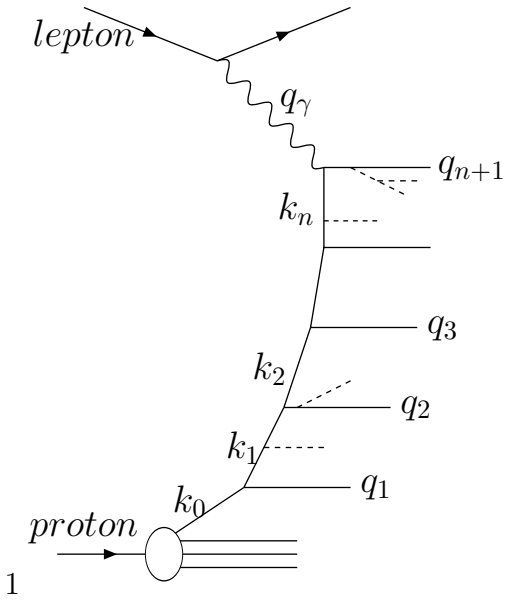

Figure 2: *A fan diagram for a DIS event. The quasireal partons from the initial state radiation are denoted q_i, and the virtual propagators k_i. The dashed lines denote final state radiation.*

chain gives a contribution ($x_i \equiv k_{+,i}/P_{+,tot}$)

$$\prod_i^n \bar{\alpha} \frac{dx_i}{x_i} \frac{dk_{\perp,i}^2}{k_{\perp,i}^2} \quad \text{where} \quad \bar{\alpha} \equiv \frac{3\alpha_s}{\pi}. \tag{2}$$

We note that this is a contribution to the "non-integrated structure function" $\mathcal{F}$, defined by

$$F(Q^2) \sim \int \mathcal{F}(k_\perp^2) d\ln(k_\perp^2). \tag{3}$$

Integrating over the appropriate integration regions and summing over possible values of n, the number of links in the chain, we readily obtain (for a fixed coupling $\bar{\alpha}$)

$$\mathcal{F} \sim \sum_n \bar{\alpha}^n \frac{(\ln 1/x)^n}{n!} \frac{(\ln Q^2)^n}{n!} \approx \exp(2\sqrt{\bar{\alpha} \ln Q^2 \ln 1/x}). \tag{4}$$

For a running coupling we get instead of $\ln Q^2$ a factor $\ln \ln Q^2$. We want to stress that to get the properties of the final state, we have to add final state emission within regions allowed by angular ordering.

For very small x and limited Q^2, the BFKL region, also non-ordered chains become important, although suppressed. Solutions to the BFKL equation [4] increase like a power $1/x^\lambda$ for small x-values. As mentioned above, for a running coupling we find that the $k_\perp$-distribution saturates for very long chains [3]. This implies that all the $k_{\perp i}$-integrals give the same constant result, and instead of eq. (4) we then obtain

$$\mathcal{F} \sim \sum_n \bar{\alpha}^n \frac{(\ln 1/x)^n}{n!} (const.)^n \sim \exp(\lambda \ln 1/x) = \frac{1}{x^\lambda}. \tag{5}$$

Such a power-like behavior, $F \sim 1/x^\lambda$, with $\lambda \sim 0.3$, is indicated in data from HERA. (We note, however, that it is also possible to describe this increase by NLO DGLAP evolution.)

In the *interpolation* region between the DGLAP and BFKL regimes we have to calculate suppressed contributions from non-ordered chains. For each chain of initial state radiation, final state emission should be added within specified kinematic regions. This final state radiation should give negligible recoils. It should also be described by Sudakov form factors, which implies that the final state emission only affects the properties of the final state and not the cross section (i. e. the reaction probability), which is described by the structure function. Thus a chain with specified initial state radiation represents a set of final states with all possible final state emissions. We want to stress that the separation between initial and final state radiation is not given by Nature, but is defined by the calculation scheme.

A specific scheme, which interpolates between the DGLAP and the BFKL results, was presented by Ciafaloni, Catani, Fiorani and Marchesini, the CCFM model [1]. In this scheme those final state gluons, which are not followed in rapidity (or angle) by a more energetic gluon, are regarded as initial state radiation, all other as final state emission. With this definition they showed that the contribution from a particular chain is given by the expression

$$\mathcal{F} \sim \sum \int \prod \bar{\alpha} \frac{dz_i}{z_i} \frac{d^2 q_{\perp,i}}{\pi q_{\perp,i}^2} \Delta_{ne}(z_i, k_{\perp,i}, q_{\perp,i}) \tag{6}$$

where $\Delta_{ne}(z_i, k_{\perp,i}, q_{\perp,i})$ is a specific non-eikonal form factor (see ref [1]).

3 The Linked Dipole Chain Model

In the Linked Dipole Chain model [2] (LDC) more gluons are treated as final state radiation. The remaining (initial state) gluons are ordered both in q_+ and in q_-. (This implies that they are also ordered in y.) Thus a single chain in the LDC model represents a set of chains in the CCFM scheme, all with the same "backbone" of harder gluons. In ref [2] it is demonstrated that if we sum over all states in this set, with their corresponding non-eikonal form factors, then all this adds up to unity. Thus the form factors are exactly canceled, and $\mathcal{F}$ can be written in the simple form

$$\mathcal{F} \sim \sum \int \prod \bar{\alpha} \frac{dz_i}{z_i} \frac{d^2 q_{\perp,i}}{\pi q_{\perp,i}^2}. \tag{7}$$

Fig. 3 shows a typical chain in a $(y, \ln q_\perp^2)$-plane. The real emitted partons q_i, are mapped onto points in this figure. The virtual propagators do not have a well defined rapidity; they are represented by horizontal lines, whose left ends correspond to the values of $k_{\perp,i}$ and $k_{+,i}$. The larger region allowed for final state radiation in the LDC model corresponds to the region below the horizontal lines in Fig. 3. It is convenient to express the result in terms of the propagator momenta k_i, using the relations $d^2 q_{\perp,i} = d^2 k_{\perp,i}$ and $q_{\perp,i}^2 \approx \max(k_{\perp,i}^2, k_{\perp,i-1}^2)$. Thus eq. (7) can be written in the form

$$\mathcal{F} \sim \sum \int \prod \bar{\alpha} \frac{dz_i}{z_i} \frac{dk_{\perp,i}^2}{\max(k_{\perp,i}^2, k_{\perp,i-1}^2)}. \tag{8}$$

This implies that for a "step up" or a "step down" in $k_\perp$ we find the following weights

$$\frac{d^2 q_{\perp,i}}{q_{\perp,i}^2} \approx \frac{d^2 k_{\perp,i}}{k_{\perp,i}^2}, \quad k_{\perp,i} > k_{\perp,i-1} \quad \text{and} \tag{9}$$

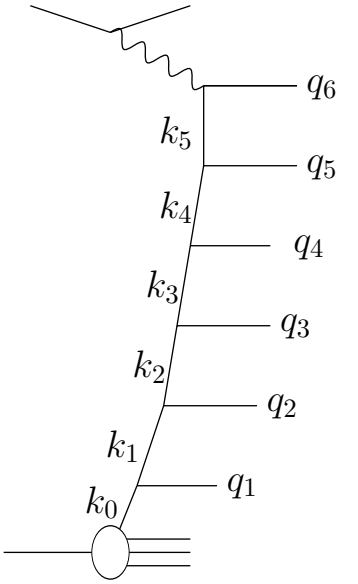

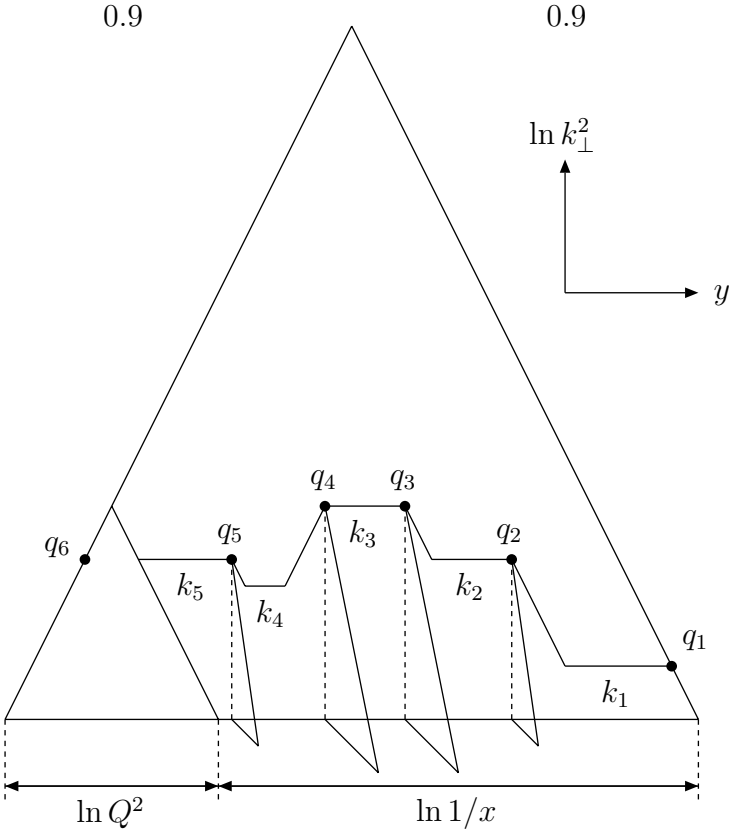

Figure 3: *The initial state emissions q_i in the $(y, \kappa = ln(k_\perp^2))$-plane. Final state radiation is allowed in the region below the horizontal lines.*

$$\frac{d^2q_{\perp,i}}{q^2_{\perp,i}} \approx \frac{d^2k_{\perp,i}}{k^2_{\perp,i}} \cdot \frac{k^2_{\perp,i}}{k^2_{\perp,i-1}}, \quad k_{\perp,i} < k_{\perp,i-1}. \tag{10}$$

Thus for a step down we have an extra suppression factor $k^2_{\perp,i}/k^2_{\perp,i-1}$. This implies that if the chain goes up to $k_{\perp max}$ and then down to $k_{\perp,final}$ we obtain the factor

$$\prod \frac{dk^2_{\perp,i}}{k^2_{\perp,i}} \cdot \frac{k^2_{\perp,final}}{k^2_{\perp max}}. \tag{11}$$

This gives a factor $1/k^4_{\perp max}$, which corresponds to a hard parton-parton subcollision.

In DIS also chains for which $k^2_{\perp,final} > Q^2$ can contribute to the cross section. These chains correspond to boson-gluon fusion events, and the definition of the structure function $F(x,Q^2)$ implies that these contributions contain a similar suppression factor $Q^2/k^2_{\perp,final}$. Thus the symbolic relation in eq. (3) can more exactly be written in the form

$$F = \int^{Q^2} \frac{dk^2_\perp}{k^2_\perp}\mathcal{F}(x,k^2_\perp) + \int_{Q^2} \frac{dk^2_\perp}{k^2_\perp}\mathcal{F}(x\frac{k^2_\perp}{Q^2},k^2_\perp)\frac{Q^2}{k^2_\perp}. \tag{12}$$

Note that in the second term, besides the suppression factor $Q^2/k^2_\perp$ we have also a shifted x-value. "Normal" chains, for which $k^2_{\perp,final} < Q^2$, end on the line AB in Fig. 4, which corresponds to $k_{+,final} = x \cdot P_{+,tot}$, but due to energy-momentum conservation, chains for which $k^2_{\perp,final} > Q^2$ end instead on the line AC, which corresponds to $k_{+,final} = x \cdot \frac{k^2_{\perp,final}}{Q^2} \cdot P_{+,tot}$.

We see that in the LDC model different types of reactions are treated in the same formalism, without double counting or missed parts of phase space. Thus Fig. 4 shows three chains representing different types of reactions:

I. "normal" DIS,
II. boson-gluon fusion: $k^2_{\perp,final} > Q^2$,
III. hard resolved photon collision: $k^2_{\perp,max} > k^2_{\perp,final} (> Q^2)$.

An essential feature of the LDC formalism is that it is fully *left-right symmetric*, meaning that the same result is obtained if the chain is generated from the photon end instead of from the proton end. Although not evident from eq. (8), this is obvious from the expression in eq. (7). This feature also means that the same formalism can be used if the (resolved) photon in one end of the chain is replaced by a hadron. In section 5 we will see that the symmetric property of the LDC formalism makes it particularly effective for an understanding of the minijet distribution in hadronic reactions or nucleus-nucleus collisions.

Before we go into more details about the properties of this minijet plateau, we want to mention some other properties of the LDC model:

- It is straight forward to allow for a running coupling α_s within the formalism.
- It is possible to include quarks and other non-leading effects (non-leading terms in the splitting functions). The result is also improved when the link with highest $p_\perp$ is adjusted to the exact matrix element.
- The chains contain only those gluons (or quarks), which cannot be regarded as final state radiation. This might be called the "backbone" of the chain, and the fact that hard jets are not yet subdivided into many sub-jets may make it more easy to study minijets and $E_\perp$-flow, and to interpret the results of the calculations.

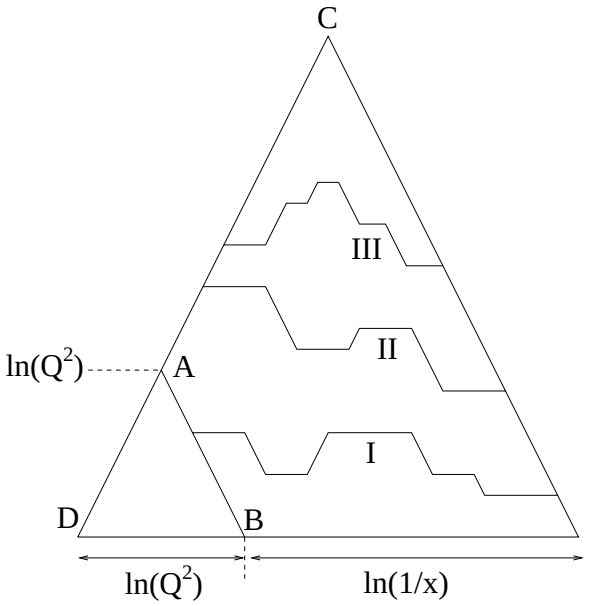

Figure 4: *Different types of parton chains. I: "Normal" DIS. II: Boson-gluon fusion. III: Hard resolved photon collision.*

- The fact that there are fewer gluons in the primary chain also implies that typical z-values are smaller, and therefore smaller sub-leading effects are expected.
- The formalism is suitable for MC simulation. Such a program is developed by Lönnblad and Kharraziha [5].

Naturally it is essential to verify that the LDC model also can reproduce experimental data. Preliminary results indicate that the LDC MC indeed is able to successfully describe experimental results, both for the structure functions and for the properties of the final states, for example the production of jets and transverse energy flow [6].

4 Integral equations and asymptotic behavior

It is straight forward to derive integral equations for the non-integrated structure function $\mathcal{F}$. From the relation in eq. (12) we obtain the equation

$$\frac{\partial \mathcal{F}(l,\kappa)}{\partial l} = \int_{\kappa_{cut}}^{\kappa} d\kappa' \bar{\alpha}(\kappa) \mathcal{F}(l,\kappa') + \int_{\kappa} d\kappa' \bar{\alpha}(\kappa') \mathcal{F}(l+\kappa-\kappa',\kappa') exp[-(\kappa'-\kappa)] \qquad (13)$$

where $l \equiv \ln(1/x)$ and $\kappa \equiv \ln k_\perp^2$.

It is well known that the BFKL formalism with a constant coupling, α_s, implies that the transverse momenta grow like a random walk in $\ln k_\perp^2$, which gives a Gaussian distribution that widens with $\ln(1/x)$, $<\ln k_\perp^2> \sim \sqrt{\ln(1/x)}$. A running coupling favors smaller $k_\perp$-values, and this implies that the $k_\perp$-distribution does not widen indefinitely, but saturates for small x [3]. The solution to eq. (13) can then be written in the factorized form

$$\mathcal{F} \approx \frac{1}{x^\lambda} \cdot f(\kappa), \quad x \text{ small.} \qquad (14)$$

The fact that small $k_\perp$-values are not suppressed implies that the value of λ is sensitive to the soft region, and some kind of cutoff has to be introduced. Thus λ cannot be determined from perturbative QCD alone, but has to be determined from experimental data. (This feature is consistent with the very large lower order corrections to the BFKL equation [7], which indicates that the perturbative series may converge badly.) This affects also the $k_\perp$-dependence described by the function f in eq. (14). The dependence on x and $k_\perp$ becomes correlated in such a way that for large $k_\perp$, f takes the asymptotic form

$$f(\kappa) \propto \kappa^{\frac{\alpha_0}{\lambda}-1}. \tag{15}$$

Actually MC calculations show that the simple power in eq. (15) is a rather good approximation, not only for large κ but for the whole κ-interval [3].

The factorized form in eq. (14) implies also that for limited Q^2 and very small x (or hadronic collisions at very high energies) a central plateau is developed in the minijet distribution. The properties of this plateau will be further studied in the next section.

5 Inclusive Jet Cross Section

The properties of the fan diagram in Fig 2 depend on the chosen separation between initial state and final state radiation. As mentioned above, the same event corresponds to a chain with fewer links in the LDC formalism than in e. g. the CCFM formalism, because in the LDC model more emissions are formally treated as final state radiation. The number of jets is not a well-defined concept, if it is not accompanied by some specification of the resolution, and two different schemes can be equally correct if one jet in one scheme corresponds to two or more sub-jets in the other. The total $E_\perp$-flow is however expected to be approximately unaffected, when one jet is split in two or several smaller jets by final state radiation. As mentioned in section 3, the LDC formalism is fully symmetric with respect to the two ends of the fan or ladder diagram, and we will see that this makes it particularly effective for a analysis of the minijet distribution. (In the CCFM formalism the fan diagram for the initial state radiation is not symmetric; the symmetry is only restored after inclusion of the final state emission.)

A long chain as in Fig. 5, with $Q^2 = Q_0^2$ and with a local maximum $k_{\perp,max} = k_{\perp,i}$, corresponds to a hard scattering between two partons with momenta k_{i-1} and $-k_{i+1}$. Due to the symmetry of the expression in eq. (7), these two pieces of the chain can be interpreted as evolution from both ends towards the central hard scattering. The momentum transfer in this hard subcollision is given by k_i, and there is a minus sign in the momentum of one of the colliding partons, as this part of the chain is regarded as evolving from the top, in the fan diagram, downwards towards $-k_{i+1}$.

A single chain may also have more than one local maximum, which corresponds to two or more correlated hard subcollisions. If we want to obtain the inclusive jet cross section, or the total $E_\perp$-flow, we have to include all produced partons q_j in the chain. To calculate this we start by studying a single link in the central part of a long chain. There are three different types of links. Besides a local maximum as in Fig. 5 and Fig. 6a, we have also the two possibilities shown in Fig. 6b and Fig. 6c. To simplify the notation we call the gluons k_a, k, and k_b as indicated in Fig. 6, and study the three cases:

1. $k_\perp > k_{\perp,a}, k_{\perp,b}$. Transverse momentum conservation implies that $q_{\perp,a} \approx q_{\perp,b} \approx k_\perp$, and it corresponds to a normal hard Rutherford scattering between two partons.

The two colliding partons have virtualities given by $k^2_{\perp,a}$ and $k^2_{\perp,b}$, which both are small compared to the exchanged momentum $k^2_\perp$. From eqs. (8-10) we see that the link is associated with the following weight factor

$$\frac{1}{k^4_\perp} \cdot \alpha_{\rm s}^2(k^2_\perp), \tag{16}$$

which corresponds to the cross section for gluon exchange between two quasireal particles.

2. $k_{\perp,b} > k_\perp > k_{\perp,a}$, which implies that $q_{\perp,a} \approx k_\perp$ and $q_{\perp,b} \approx k_{\perp,b}$. From eq. (9) we see that instead of the expression in eq. (16), this link is associated with the following weight

$$\frac{1}{k^2_\perp \cdot k^2_{\perp,b}} \cdot \alpha_{\rm s}(k^2_\perp) \cdot \alpha_{\rm s}(k^2_{\perp,b}). \tag{17}$$

A similar result is obtained for $k_{\perp,a} > k_\perp > k_{\perp,b}$.

3. $k_\perp < k_{\perp,a}, k_{\perp,b}$, in which case $q_{\perp,a} \approx k_{\perp,a}$ and $q_{\perp,b} \approx k_{\perp,b}$. The corresponding weight is now given by

$$\frac{1}{k^2_{\perp,a} \cdot k^2_{\perp,b}} \cdot \alpha_{\rm s}(k^2_{\perp,a}) \cdot \alpha_{\rm s}(k^2_{\perp,b}). \tag{18}$$

We see that when $k_\perp$ is less than $k_{\perp,a}$ or $k_{\perp,b}$, one factor $1/k^2_\perp$ is replaced by $1/k^2_{\perp,a}$ or $1/k^2_{\perp,b}$ respectively. As will be discussed more in the following, this implies that the inclusive cross section becomes non-singular for small transverse momenta.

Keeping k_a, k, and k_b fixed, we note that integrating and summing over all partons to the right of the link corresponds exactly to the non-integrated structure function $\mathcal{F}(x_a, k^2_{\perp,a})$, where x_a is the Bjorken variable, i. e. the scaled positive lightcone momentum, $x_a = k_{+,a}/P_{+,tot}$. Similarly, integration and summation of partons to the left of the link gives $\mathcal{F}(x_b, k^2_{\perp,b})$, with x_b the corresponding scaled negative lightcone momentum $x_b = x_b^{(-)} = -k_{-,b}/P_{-,tot}$.

The inclusive jet distribution can then be written in the form ($\hat{s}$ is the Mandelstam variable for the hard subcollision)

$$\begin{aligned}\frac{d\sigma_{incl}}{dq^2_\perp dy} \propto \int \frac{dx_a}{x_a} \cdot \frac{dx_b}{x_b} \cdot \frac{dk^2_{\perp,a}}{k^2_{\perp,a}} \cdot \frac{dk^2_{\perp,b}}{k^2_{\perp,b}} \cdot \mathcal{F}(x_a, k^2_{\perp,a}) \cdot \mathcal{F}(x_b, k^2_{\perp,b}) \\ \cdot \frac{1}{2} \cdot \frac{d\hat{\sigma}}{dq^2_\perp}(q^2_\perp, k^2_{\perp,a}, k^2_{\perp,b}, \hat{s} = x_a x_b s) \cdot \delta(y - \frac{1}{2}\ln\frac{x_a}{x_b}).\end{aligned} \tag{19}$$

In this formalism each produced parton is counted in two different links, one to the left and one to the right. In our notation $\frac{d\hat{\sigma}}{dq^2_\perp}$ is the inclusive cross section counting both emitted partons, and therefore a factor $\frac{1}{2}$ is needed to avoid double counting. The cross section $\frac{d\hat{\sigma}}{dq^2_\perp}$ is obtained by integrating eqs. (16-18) over $k^2_\perp$ with the constraint $k^2_\perp < \hat{s}$. In case 1 above we will then get the integral (for $k_{\perp,b} > k_{\perp,a}$)

$$\int_{k^2_{\perp,b}}^{\hat{s}} dk^2_\perp \cdot \frac{1}{k^4_\perp} \cdot 2 \cdot \delta(q^2_\perp - k^2_\perp) = \frac{2}{q^4_\perp} \cdot \theta(q^2_\perp - k^2_{\perp,b}) \cdot \theta(\hat{s} - q^2_\perp). \tag{20}$$

Here the factor 2 in front of the δ-function originates from the fact that we count both $q^2_{\perp,a}$ and $q^2_{\perp,b}$, each being approximately equal to $k^2_\perp$. The contributions from cases 2 and

3 can be calculated in the same way. If we, for clarity, first neglect the running of α_s, we find (again for $k_{\perp,b} > k_{\perp,a}$)

$$\begin{aligned}\frac{d\hat{\sigma}}{dq_\perp^2} &\propto \alpha_s^2 \left\{ \frac{2}{q_\perp^4} \cdot \theta(q_\perp^2 - k_{\perp,b}^2) \cdot \theta(\hat{s} - q_\perp^2) + \right. \\ &+ \frac{1}{q_\perp^2 \cdot k_{\perp,b}^2} \cdot \theta(q_\perp^2 - k_{\perp,a}^2) \cdot \theta(k_{\perp,b}^2 - q_\perp^2) + \delta(q_\perp^2 - k_{\perp,b}^2) \cdot \frac{1}{k_{\perp,b}^2} \cdot \ln \frac{k_{\perp,b}^2}{k_{\perp,a}^2} + \\ &+ \left. \left[\delta(q_\perp^2 - k_{\perp,b}^2) + \delta(q_\perp^2 - k_{\perp,a}^2) \right] \cdot \left[\frac{1}{k_{\perp,b}^2} - \max\left(\frac{1}{\hat{s}} \, , \, \frac{k_{\perp,cut}^2}{k_{\perp,a}^2 k_{\perp,b}^2} \right) \right] \right\}. \end{aligned} \tag{21}$$

Here the first line corresponds to a "normal" hard subcollision, case 1 above. The second line corresponds to case 2, where one of the colliding partons has a virtuality larger than the exchanged momentum $-\hat{t} = k_\perp^2$, and the third line to case 3 where both initial partons have high virtualities. Note that if we have a soft cutoff $k_{\perp,cut}^2$, the lower limit in the $k_\perp^2$-integral for case 3 is given by $\max(\frac{k_{\perp,a}^2 k_{\perp,b}^2}{\hat{s}}, k_{\perp,cut}^2)$.

The inclusive jet cross section is now readily obtained from inserting eq. (21) into eq. (19) and integrating with respect to $x_a, x_b, k_{\perp,a}$ and $k_{\perp,b}$. Due to the factorized form $\mathcal{F}(x,\kappa) \approx x^{-\lambda} \cdot f(\kappa)$ in eq. (14), with a power-like dependence on x, the result is independent of the rapidity of the pair, $y = \frac{1}{2} ln \frac{x_a}{x_b}$, for fixed value of $x_a \cdot x_b = \hat{s}/s$. Thus the distribution corresponds to a central plateau with a height proportional to $(x_1 \cdot x_2)^{-\lambda}$, which for fixed $\hat{s}$ grows with energy proportional to s^λ.

The integration is straight forward if we assume the power-like approximation for $f(\kappa)$ in eqs. (14-15), $\mathcal{F}(x,\kappa) \approx x^{-\lambda} \cdot f(\kappa) \propto x^{-\lambda} \kappa^{\frac{\alpha_0}{\lambda} - 1}$. As an example, for the term in eq. (20) (the first term in eq. (21)) the integral over x_a and x_b gives

$$\int \frac{dx_a}{x_a} \frac{dx_b}{x_b} \delta(y - \frac{1}{2} \ln \frac{x_a}{x_b}) \cdot \frac{1}{(x_a x_b)^\lambda} = \int_{q_\perp^2} \frac{d\hat{s}}{\hat{s}} \left(\frac{s}{\hat{s}} \right)^\lambda = \frac{1}{\lambda} \left(\frac{s}{q_\perp^2} \right)^\lambda \tag{22}$$

while the integral over $k_{\perp,a}$ and $k_{\perp,b}$ gives (including also the symmetric case $k_{\perp,a}^2 > k_{\perp,b}^2$)

$$\alpha_s^2(q_\perp^2) \int^{\ln q_\perp^2} d\kappa_b \cdot \kappa_b^{\frac{\alpha_0}{\lambda} - 1} \int^{\ln q_\perp^2} d\kappa_a \cdot \kappa_a^{\frac{\alpha_0}{\lambda} - 1} = \alpha_s^2(q_\perp^2) \cdot \left[\frac{\lambda}{\alpha_0} \kappa^{\frac{\alpha_0}{\lambda}} \right]^2. \tag{23}$$

The full result is, however, rather lengthy, if we take into account the running coupling α_s, and we write it in the form

$$\frac{d\sigma_{incl}^{jet}}{dq_\perp^2 dy} \propto \frac{s^\lambda}{q_\perp^{4+2\lambda}} \cdot \alpha_s^2(q_\perp^2) \cdot h(q_\perp^2). \tag{24}$$

The factor $s^\lambda / q_\perp^{2\lambda}$ is a consequence of the increase of $\mathcal{F} \sim x^{-\lambda}$ for small x (cf eq. (14)), and we have also extracted a factor $\alpha_s^2(q_\perp^2)$. Thus the function $h(q_\perp^2)$ is defined in such a way, that it would be constant in the unrealistic case, where the parton flux is given by a scaling function $F(x) \sim 1/x^\lambda$, which is independent of Q^2. The result in eq. (24) is proportional to s^λ, but we emphasize that this is the growth of the cross section for jet production, and not the number of jets per event.

The transverse momentum dependence of the function $h(q_\perp^2)$ for a running α_s is shown by the solid line in Fig. 7. (We have here assumed $\lambda = 0.3$.) Also shown in this figure is the contribution from "normal hard subcollisions", i. e. partons associated to a local

maximum in the $k_\perp$ chain. We see that this contribution dominates for large $q_\perp^2$, while for smaller $q_\perp^2$, the partons which are not associated to a local maximum play a more important role, contributing more than 40% for $q_\perp^2 < 5\,\mathrm{GeV}^2$. For large $q_\perp^2$, $h(q_\perp^2)$ behaves as a power of $\ln q_\perp^2$, which corresponds to the scaling violation in the structure functions. For smaller $q_\perp^2$, $h(q_\perp^2)$ is essentially linear in $q_\perp^2$. This implies that the total transverse energy flow $dE_\perp/dy = \frac{1}{\sigma_{tot}} \cdot \int \frac{d\sigma}{dq_\perp^2 dy} dq_\perp^2 \cdot q_\perp$ is convergent for small $q_\perp$. Consequently the $E_\perp$ distribution is limited also without a low $q_\perp$ cutoff. In Fig. 7a we also show the $q_\perp$-dependence obtained from the MC (normalized to the same total flow), and we see a very nice agreement with our analytic result.

We note that although "normal hard collisions" dominate for large $q_\perp$, the other contributions correspond to approximately 25% even for $q_\perp^2 \approx 1000\,\mathrm{GeV}^2$. We expect that most of this difference would be accounted for in a calculation where hard collisions are calculated to next-to-leading order, including also $2 \to 3$ parton reactions, which thus can take into account one extra parton. This approach would, however not solve the problems encountered for small or medium $q_\perp$.

In the literature the inclusive jet cross section is often estimated from a product of two (integrated) structure functions $F(x, q_\perp^2)$ and a hard subcollision cross section $\frac{d\hat{\sigma}}{dq_\perp^2}$ for quasireal colliding partons. This estimate can be written in the form

$$\begin{aligned} \frac{d\sigma_{incl}^{jet}}{dq_\perp^2 dy} &\propto \int \frac{dx_a}{x_a}\frac{dx_b}{x_b}\delta(y - \frac{1}{2}\ln\frac{x_a}{x_b}) \cdot F(x_a, q_\perp^2) \cdot F(x_b, q_\perp^2) \cdot \frac{1}{q_\perp^4} \cdot \alpha_s^2(q_\perp^2) \propto \\ &\propto \frac{1}{q_\perp^{4+2\lambda}} \cdot \alpha_s^2(q_\perp^2) \cdot h_{naive}(q_\perp^2). \end{aligned} \tag{25}$$

Here the function h_{naive} is defined analogously to the function h in eq. (24).

It is interesting to compare this "naive" estimate with our result in eq. (24). The relation between $F(x, q_\perp^2)$ and the non-integrated structure function $\mathcal{F}(x, k_\perp^2)$ is shown in eq. (12). There are two contributions to F, one (ordered) contribution with $q_\perp > k_\perp$, and another suppressed contribution with $q_\perp < k_\perp$. When one or both colliding partons are virtual, there is a suppression factor $q_\perp^2/k_{\perp,a}^2$ and/or $q_\perp^2/k_{\perp,b}^2$. With a cross section assumed to be proportional to $\frac{\alpha_s^2(q_\perp^2)}{q_\perp^4}$ as in eq. (24), we see that each link is given just the weight presented in eq. (16), eq. (17), or eq. (18). The difference lies in the fact that in eq. (25) both outgoing partons are assumed to have transverse momenta given by the momentum transfer in the collision. This underestimates the $q_\perp$ for collisions corresponding to the links in Fig. 6b and Fig. 6c. This underestimate is compensated by the fact that every link in the fan diagram corresponds to a hard collision in eq. (25). Thus this equation corresponds to two produced partons per link instead of one. This double counting does not give a full factor of two, due to the underestimate of the $q_\perp$ mentioned above. The result is illustrated in Fig. 8. The really emitted partons in a chain are marked by a dot, while the naive expression in eq. (25) corresponds to a final state parton at every point marked by a circle. Thus in the naive calculation only the partons at a local maximum are given their proper weight. Those at a minimum value for $k_\perp$ should not be included at all, as no real emitted partons have these $k_\perp$-values, and those in-between are counted twice.

For a quantitative estimate of the jet cross section and a comparison with the "naive" approach, it would be suitable to use a Monte Carlo, which can take into account also effects from non-asymptotic energy, non-leading terms in the parton-parton cross section and contributions from quarks. However, we believe that the qualitative features can be

understood from an approximate analytic calculation, provided the same approximations are used in both approaches. Thus for $F(x,q_\perp^2)$ and $\mathcal{F}(x,k_\perp^2)$ we use the relations in eq. (12) and eqs. (14-15). We study purely gluonic chains and for the subcollision we use the leading expression $\frac{d\hat{\sigma}}{dq_\perp^2} \propto \frac{\alpha_s^2(q_\perp^2)}{q_\perp^4}$.

Fig. 9 shows the ratio $h(q_\perp^2)/h_{naive}(q_\perp^2)$ as a function of the transverse momentum (note the logarithmic $q_\perp$-scale). For large $q_\perp$ the Rutherford contribution dominates in both cases, making $h(q_\perp^2) \approx h_{naive}(q_\perp^2)$. For smaller $q_\perp$, on the other hand, the naive expectation gives a significant overestimate. This can also be concluded from Fig. 10, which shows the distribution in transverse energy, $dE_\perp/dydq_\perp^2 = q_\perp \cdot dn/dydq_\perp^2$. We see that the total $E_\perp$ in the minijet region, $q_\perp \lesssim 5$ GeV, is almost a factor 2 larger in the naive estimate. It is often realized that this large contribution for very low $q_\perp$ must be unphysical, and therefore a soft cutoff, $q_{\perp min}$, is introduced in many calculations. This cutoff is often assumed to be around 2 GeV and slowly growing with energy (see e.g. [8]). In Fig 11 we show the integrated transverse energy $\int^{q_\perp^2} dq_\perp^2 \frac{dE_\perp}{dydq_\perp^2}$. From this figure we see that

$$\int^{\infty} dq_\perp^2 \left.\frac{dE_\perp}{dydq_\perp^2}\right|_{our\,result} \approx \int_{q_{\perp min}^2}^{\infty} dq_\perp^2 \left.\frac{dE_\perp}{dydq_\perp^2}\right|_{naive} \tag{26}$$

for $q_{\perp min} \approx 2.1$ GeV. This means that for asymptotic energies the total $E_\perp$ in our approach equals the naive result when $q_{\perp min} \approx 2.1$ GeV. For smaller energies the maximal value of $q_\perp$ is limited, which implies that a somewhat smaller value of $q_{\perp min}$ is needed. A reliable quantitative estimate would need a calculation which includes quark jets and non-leading contributions, which could be obtained with the help of the MC program. We note in particular that in our approach the corresponding effective cutoff of the naive approach, $q_{\perp min}$, saturates for very large energies. In the conventional approach it is difficult to make predictions for higher energies without a physical understanding of the energy dependence of $q_{\perp min}$.

Only for comparison, we have in Fig. 10 also included the distribution one would obtain from eq. (24) if the structure function F were scaling and independent of $q_\perp^2$. (The normalization is adjusted to our result for large momenta.) As is seen, this would give a very much larger (and totally unrealistic) increase for small $q_\perp$.

We end this section by noting that one chain forms a set of correlated jets. The fact that the $k_\perp$-distribution saturates for long chains (cf eq. (14)) implies that not only the $p_\perp$ of the jets, but also their density (the number of jets per unit rapidity) is independent of the length of the chain, i. e. independent of the energy in the collision. The jet density grows because the number of possible chains increases proportional to s^λ. It is also conceivable that the number of chains is not random, but e. g. correlated with the impact parameter, so that central collisions have more and peripheral collisions fewer chains [9]. In this paper we have only studied the average jet multiplicity, and we postpone the study of different types of correlations to future investigations.

The possible correlation between different chains may also affect the total cross section. We want to stress that the results in eq. (24) correspond to the cross section for jet production. To find the number of jets per event we have to divide by the total cross section, which is not directly obtained from our formulae.

6 Conclusions

A good understanding of jet and minijet production, and transverse energy flow, is essential for a proper interpretation of new phenomena in pp collisions at LHC or a possible formation of a quark-gluon plasma in nucleus collisions at RHIC or LHC. For very high $p_\perp$ the parton flux can be described by DGLAP ($k_\perp$-ordered) evolution. The large momentum transfer between the colliding partons implies that the two evolving chains are independent of each other. For moderate and smaller $p_\perp$ (and high energies) we enter the BFKL regime and non-ordered chains become important. Here it is essential to take coherence effects and correlations into account. As we can then have several hard subcollisions in a single chain or ladder diagram, it is also important to avoid double counting.

The parton evolution in the BFKL regime can be described by the CCFM formalism. The LDC model is a reformulation and generalization of this formalism, and the symmetric structure of the LDC model makes it particularly suited for a description of (mini)jet production. We show in this paper how the jet cross section can be properly described in terms of the non-integrated structure functions and a subcollision cross section, which is suppressed when the momentum transfer is smaller than the virtuality of the colliding partons. The result is a dynamical suppression of small-$p_\perp$ jets, which removes the strong sensitivity to a low-$p_\perp$ cutoff in traditional estimates.

7 Acknowledgments

We want to thank Bo Andersson and Leif Lönnblad for valuable discussions, and Lönnblad for help with the Monte Carlo simulations.

References

[1] M.Ciafaloni, Nucl.Phys. **B296** (1988) 49;
S.Catani, F.Fiorani and G.Marchesini, Phys.Lett. **B234** (1990) 339; Nucl.Phys. **B336** (1990) 18.

[2] B.Andersson, G.Gustafson, J.Samuelsson, Nucl. Phys. **B467** (1996) 443.

[3] B.Andersson, G.Gustafson, H.Kharraziha, Phys.Rev. **D57** (1998) 5543.

[4] E.A.Kuraev, L.N.Lipatov and V.S.Fadin, Zh.Eksp.Teor.Fiz. **72** (1977) 373 [Sov.Phys.JETP **45** (1977) 199];
Ya.Ya. Balitsky and L.N.Lipatov, Yad.Fiz. **28** (1978) 1597 [Sov.J.Nucl.Phys. **28** (1978) 822].

[5] H.Kharraziha and L.Lönnblad, Lund preprint, LUTP 97-34;
H.Kharraziha and L.Lönnblad, JHEP **03** (1998) 006.

[6] H.Jung, L.Lönnblad, Proceedings of the UK Phenomenology Workshop, Durham, Sept. 1999.

[7] V.S.Fadin and L.N.Lipatov, Phys.Lett. **B429** (1998) 127;
G.Camici and M.Ciafaloni, Phys.Lett. **B430** (1998) 349.

[8] T.Sjöstrand, Lund preprint, LUTP 99-42.

[9] T.Sjöstrand and M.van Zijl, Phys.Rev. **D36** (1987) 2019.

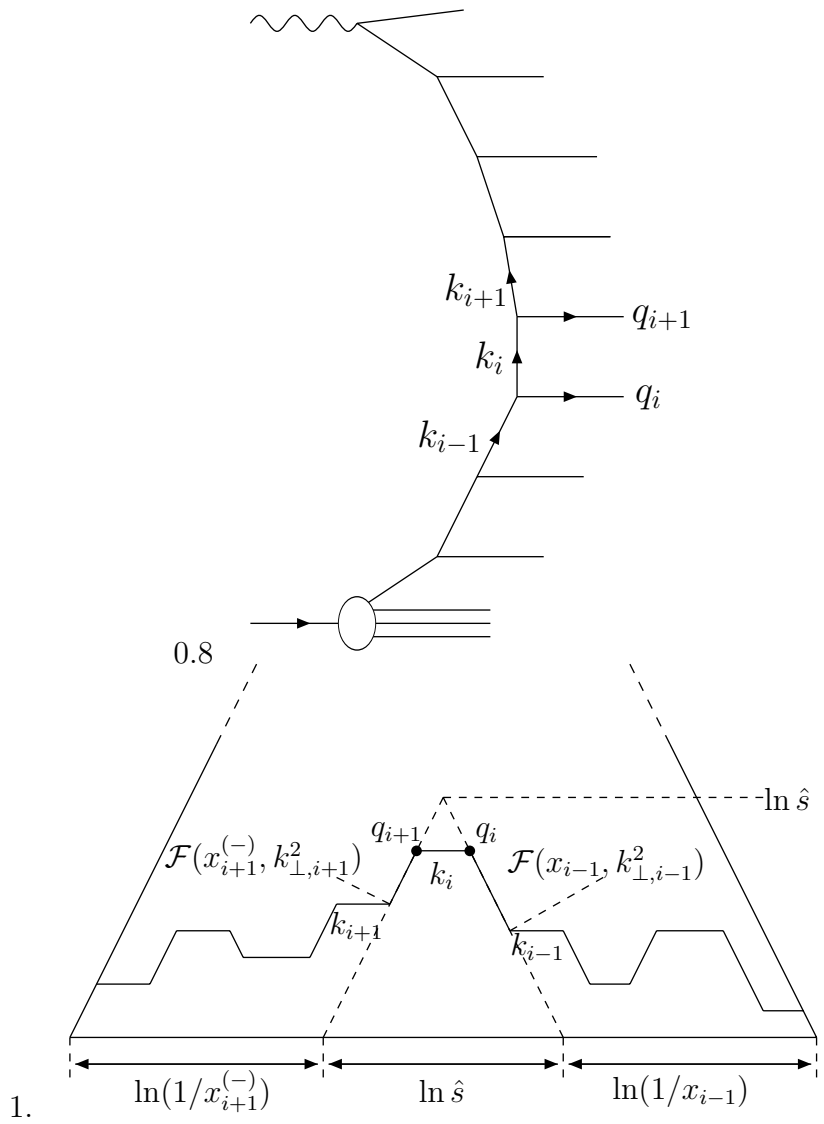

Figure 5: *A local maximum transverse momentum, $k_{\perp,max} = k_{\perp,i}$, in a long chain, corresponds to a hard subcollision between partons with momenta k_{i-1} and $-k_{i+1}$. x_i and $x_i^{(-)}$ are defined as $x_i \equiv k_{+,i}/P_{+,tot}$ and $x_i^{(-)} \equiv -k_{-,i}/P_{-,tot}$ respectively.*

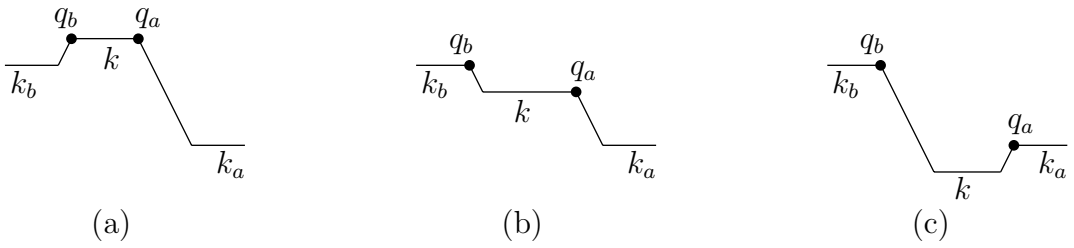

Figure 6: *The three different possibilities for a link.*

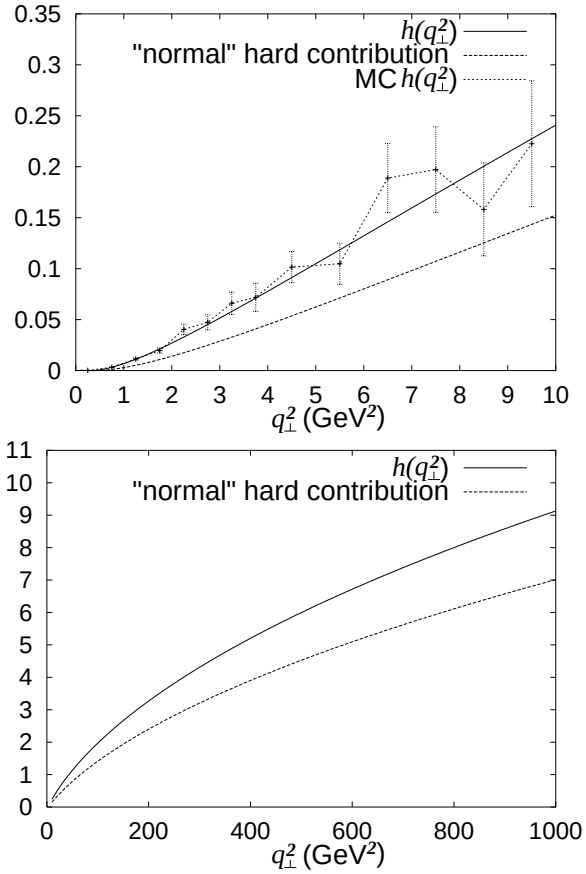

(a) (b)

Figure 7: *The transverse momentum distribution of $h(q_\perp^2)$ for (a) $q_\perp^2 < 10$ GeV^2 and (b)$q_\perp^2 < 1000$ GeV^2 according to analytical calculations (continuous curves) and MC simulation (short-dashed line).(The error bars are the estimated statistical uncertainties.) Also shown is the contribution from "normal hard subcollisions" (long-dashed line). The scale is arbitrary.*

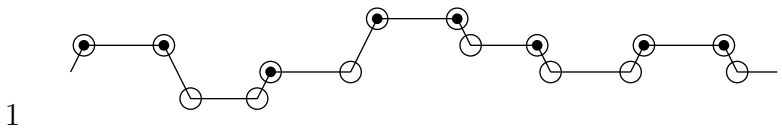

1

Figure 8: *The outgoing partons according to a correct formalism (dots) and according to a naive approach (circles).*

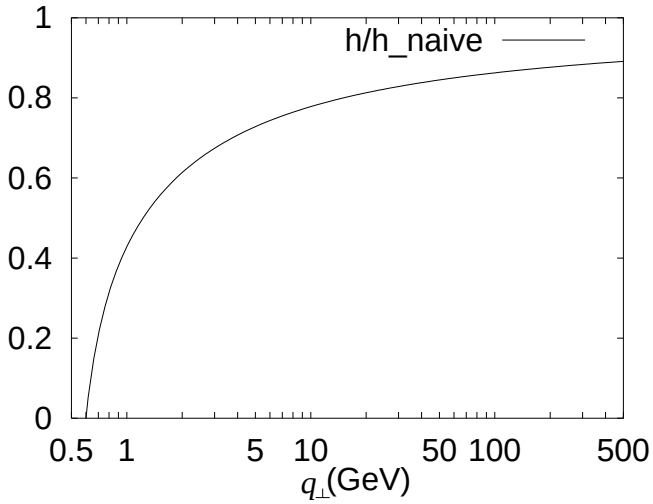

Figure 9: *The ratio $h(q_\perp^2)/h_{naive}(q_\perp^2)$ between the cross section in our approach and the naive expectation in eq. (25), as a function of $q_\perp$. (Note the logarithmic scale on the x-axis.)*

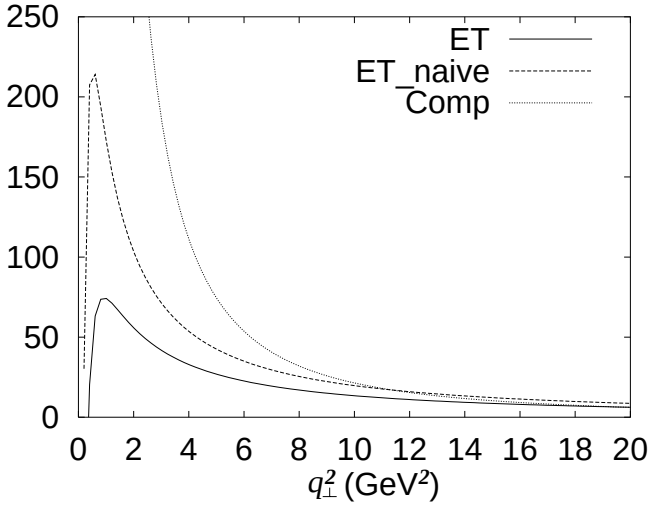

Figure 10: *Transverse energy distribution, $dE_\perp/dydq_\perp^2$, according to our calculations (continuous curve) and the "naive" estimate in eq. (25) (dashed curve). For comparison we also show the result from scaling structure functions, $F(x)$ independent of $q_\perp^2$ (dotted curve). The normalization is arbitrary.*

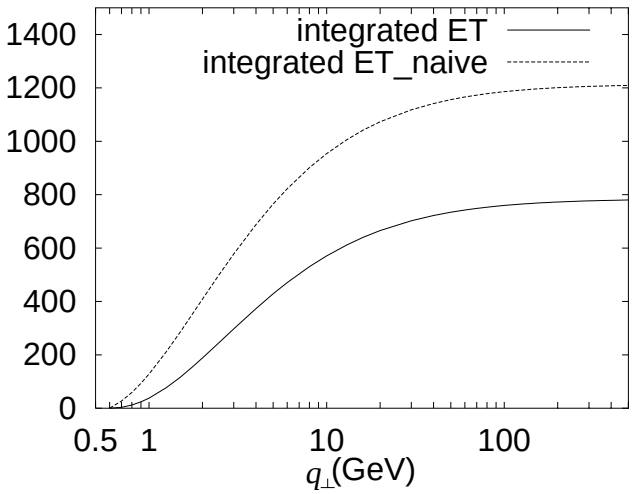

Figure 11: *Integrated transverse energy distribution, $\int^{q_\perp^2} dq_\perp^2 dE_\perp/dydq_\perp^2$, according to our calculations (continuous curve) and the "naive" estimate in eq. (25) (dashed curve). The normalization is as in Fig. 10.*